Published in final edited form as:

Biochim Biophys Acta Biomembr. 2022 October 01; 1864(10): 183974. doi:10.1016/j.bbamem.2022.183974.

Comparing the Structural Dynamics of the Human KCNE3 in Reconstituted Micelle and Lipid Bilayered Vesicle Environments

Conner Campbell[§], **Fathima Dhilhani Mohammed Faleel**[‡], **Matthew W. Scheyer**[§], **Samuel Haralu**[§], **Patrick L. Williams**[§], **William David Carbo**[§], **Aliyah Sharde Wilson-Taylor**[§], **Nima H. Patel**[§], **Charles R. Sanders**[Δ], **Gary A. Lorigan**[‡], **Indra D. Sahu**[§,‡,*]

[§] Natural Science Division, Campbellsville University, Campbellsville, Kentucky.

[‡] Department of Chemistry and Biochemistry, Miami University, Oxford, Ohio.

[Δ] Department of Biochemistry and Center for Structural Biology, Vanderbilt University, Nashville, Tennessee.

Abstract

KCNE3 is a single transmembrane protein of the KCNE family that modulates the function and trafficking of several voltage-gated potassium channels, including KCNQ1. Structural studies of KCNE3 have been previously conducted in a wide range of model membrane mimics. However, it is important to assess the impact of the membrane mimics used on the observed conformation and dynamics. In this study, we have optimized a method for the reconstitution of the KCNE3 into POPC/POPG lipid bilayer vesicles for electron paramagnetic resonance (EPR) spectroscopy. Our CD spectroscopic data suggested that the degree of regular secondary structure for KCNE3 protein reconstituted into lipid bilayered vesicle is significantly higher than in DPC detergent micelles. Electron paramagnetic resonance (EPR) spectroscopy in combination with site-directed spin labeling (SDSL) was used to probe the structural dynamics of S49C, M59C, L67C, V85C, and S101C mutations of KCNE3 in both DPC micelles and in POPC/POPG lipid bilayered vesicles. Our CW-EPR power saturation data suggested that the site S74C is buried inside the lipid bilayered membrane while the site V85C is located outside the membrane, in contrast to DPC micelle results. These results suggest that the KCNE3 micelle structures need to be refined using data obtained in the lipid bilayered vesicles in order to ascertain the native structure of KCNE3. This work will provide guidelines for detailed structural studies of KCNE3 in a more native membrane environment and comparing the lipid bilayer results to the isotropic bicelle structure and to the KCNQ1-bound cryo-EM structure.

Graphical Abstract

[*]Corresponding Author. idsahu@campbellsville.edu.

The authors declare no competing financial interest.

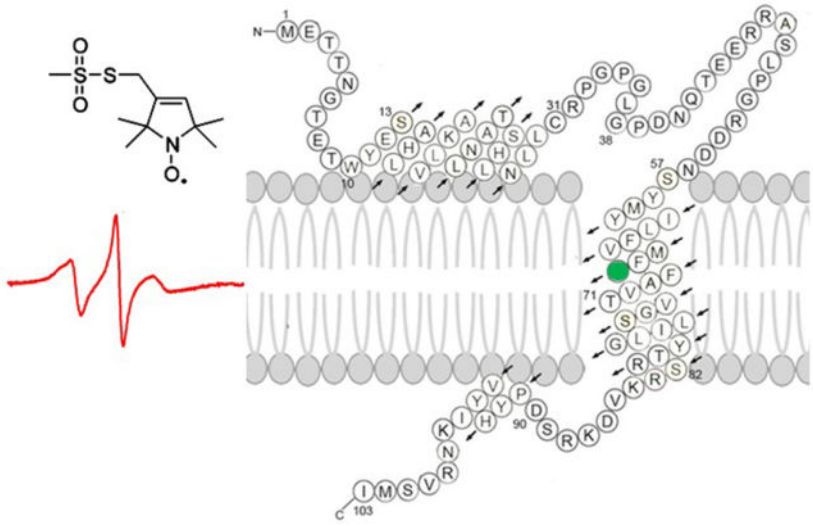

Keywords

Membrane protein; KCNE3; EPR Spectroscopy; EPR Lineshape Analysis; EPR Power saturation; Structural Dynamics

Introduction

KCNE3 is a single transmembrane protein of the KCNE family that modulates the function and trafficking of several voltage-gated potassium channels, including KCNQ1 (Q1), and KCNQ4 (1–4). Voltage-gated K^+ channels are critical for the function of cardiac, nervous and auditory systems and represent promising targets for various therapeutic agents (5, 6). KCNE3 interacts with voltage-gated K^+ channels to modulate their biophysical properties and physiological roles (3, 7). KCNE3 interacts with KCNQ1 and produces KCNE3/KCNQ1 channels that are voltage-independent in the physiological voltage range and are important for transport of potassium ions across epithelial cells as part of salt homeostasis (3, 7) and may also play a role in the cardiac action potential (8). The dysfunction of the KCNQ1/KCNE3 channel may reduce repolarizing potassium currents in the myocardium leading to the prolongation of the QT interval (8). Mutations in KCNE3 have been reported to contribute to several disorders such as long QT syndrome (LQTS), cardiac arrythmia, Brugada syndrome, cystic fibrosis and secretory diarrhea, periodic paralysis, tinnitus, and ménière's disease (1, 8–14). Despite the biological significance of KCNE3, structural dynamics and topology studies of KCNE3 in a lipid bilayer membrane have been limited.

Recently, the structure of KCNE3 was determined in isotropic bicelles (DHPC/DMPG, lipid to protein ratio (q)=0.33) using solution NMR spectroscopy by Sanders Lab (3). This structure consists of a curved α-helical transmembrane domain (TMD) with curvature being most significant close to the C-terminal end of the helical TMD, and an extracellular surface associated amphipathic helix in N-terminal, and a short juxtamembrane helix connected by a disordered region in C-terminus (3). Further, double electron electron resonance (DEER) distance measurements on a pair of spin labeled sites at the KCNE3 TMD termini in LMPC

micelles, DMPG/DHPC isotropic bicelles and POPC/POPG lipid bilayers suggested the TMD curvature is maintained in detergent micelles, bicelles, and lipid bilayers as an intrinsic property of KCNE3 (3). A recent cryo-electron microscopic (Cryo-EM) spectroscopic study on the KCNE3 complexed with KCNQ1 in the detergent micelles suggested a deviation from the independent KCNE3 structure model in isotropic bicelles with an root mean square deviation (RMSD) of 7.6 Å between the two structures (15). This study further suggested the KCNE3 pushes its TMD helix against KCNQ1 to stabilize the up conformation of the voltage sensor, locking it in its “open” configuration (15). A recent functional studies suggested that the KCNE3 mutants F68A, V72A and I76A impair the interaction between KCNQ1 and KCNE3 and shift the equilibrium of the S4 segment of the KCNQ1 to the down position (16). The structure of a membrane protein can be very different in a lipid bilayer environment when compared to a micelle/isotropic bicelles. The differences are due to the incorporation of the protein into the membrane as opposed to the micelle/isotropic bicelles due to the curved surface, hydration differences, and the inadequate hydrophobic environment. Some membrane proteins have been shown to lose function when solubilized in detergent micelles (17–19). Previous studies have further suggested that the helices in N- and C-termini undergo dynamic interaction with the membrane surface.(3) Therefore, it is very essential to understand how different segments of KCNE3 interact with lipid bilayers.

In this work, we report biophysical data on KCNE3 reconstituted into both POPC/POPG liposomes and DPC micelles. Circular dichroism (CD) and site-directed spin labeling EPR spectroscopy (SDSL-EPR) reveal differences in the mobility and conformation of KCNE3.

MATERIALS AND METHODS

Site-directed Mutagenesis

The His-tag expression vectors (pET-16b) encoding a cysteine-less mutant of KCNE3 were transformed into XL10-Gold *Escherichia coli* cells (Agilent). A QIAprep Spin Miniprep Kit (Qiagen) was used to extract the plasmid from these cells. Site-specific cysteine mutants were introduced into the cysteine-less KCNE3 gene using the QuickChange Lightning Site-Directed Mutagenesis kit (Agilent). The KCNE3 mutations were confirmed by DNA sequencing from XL10-Gold *E. coli* (Stratagene) transformants using the T7 primer (Integrated DNA Technologies). Successfully mutated vectors were transformed into *E. coli* BL21 (DE3) RP Codon-Plus competent cells for protein overexpression. Single spin label mutants (S49C, M59C, L67C, S74C, V85C, and S101C) were generated by introducing Cys residues at the positions 49, 59, 67, 85, and 101. These mutants were chosen to span the N-terminal region, transmembrane domain (TMD), and C-terminal region of KCNE3.

Overexpression and Purification

The overexpression and purification of BL21 (DE3) RP Codon-Plus *E.coli* cells containing mutated KCNE3 genes were carried out by following a protocol similar to that described previously (20). BL21 (DE3) RP Codon-Plus *E.coli* cells carrying the mutants of choice were grown in LB (Luria-Bertani) medium with 100 μg/mL ampicillin and 50 μg/ml chloramphenicol. The cell culture was incubated at 37 °C and 240 rpm until the OD_{600} reached ~0.8. The cell culture was induced using 1 mM IPTG (isopropyl-1-thio--D-

galactopyranoside), followed by continued rotary shaking at 37°C for 16 hr. Cells were harvested by centrifugation of the cultures at 6500 rpm, for 20 minutes at 4°C. The cell pellets were resuspended in 20 mL lysis buffer (70 mM Tris-HCl, pH 7.8, 300 mM NaCl) per gram of wet pellet, with 1 mM TCEP, lysozyme (0.02 mg/mL), DNase (0.02 mg/mL), RNase (0.02 mg/mL), PMSF (0.2 mg/mL), and magnesium acetate (5 mM) and tumbled at 4°C for 1 hr. The cell suspension was then subjected to sonication for 20 minutes (5 sec on/off cycles, 10 minutes total on time, Fisher Scientific Sonic Dismembrator Model 500, amplitude 40%) on ice. The lysate was centrifuged at 20,000 ×g for 30 min at 4°C and the pellet containing inclusion body was homogenized with suspension buffer (8 M urea, 25 mM Tris-HCL, 150 mM NaCl, pH 8.0, 1 mM TCEP and 0.2% sodium dodecyl sulfate (SDS) detergent) and rotated overnight at room temperature to solubilize inclusion bodies. After detergent solubilization, the insoluble debris was removed by centrifugation at 20,000 ×g for 30 minutes at 24°C. The supernatant was incubated with pre-equilibrated Ni(II)-NTA superflow resin (Qiagen) in suspension buffer for 3 hr at room temperature. The protein was then purified using the gravity flow column by washing with 10–12 bed volumes of rinse buffer (25 mM Tris-HCl, 200 mM NaCl, 0.2% SDS, 1 mM TCEP, pH 8.0) to remove non-specific proteins. Resin with bound protein was further washed with 5–6 bed volumes of exchange-rinse buffer (25 mM Tris-HCl, 200 mM NaCl, 0.1% LMPG, 1 mM TCEP, pH 8.0) to produce LMPG micelle samples. Purified His-tagged KCNE3 was eluted in 8 mL of elution buffer (25 mM Tris-HCl, 200 mM NaCl, 250 mM imidazole, 0.1% LMPG, 2 mM TCEP, pH 7.0). Protein samples were concentrated using a Microcon YM-3 (molecular weight cutoff, 3,000) filter (Amicon). The protein concentration was determined from the A_{280} using an extinction coefficient of 1.2 mg/mL protein per OD_{280} on a NanoDrop 200c (Thermo Scientific). Sodium Dodecyl Sulfate Polyacrylamide Gel Electrophoresis (SDS-PAGE) was used to assess the protein purity following purification.

Spin Labeling

MTSL spin labeling was carried out following the protocol previously published (3). After purification, each cysteine mutant was concentrated to 0.25 mM. The 2.5 mM DTT was mixed with the samples with gentle agitation at room temperature for 24 hours to ensure complete conversion to Cys-SH. 1-oxyl-2,2,5,5-tetramethylpyrroline-3-methylmethanethiosulfonate (MTSL) spin label was added to 10 mM from a 250 mM stock solution in methanol into 0.5 mM KCNE3 solution, which was then equilibrated at room temperature for 30 minutes, followed by incubation at 37°C for 3 hours and further incubated overnight at room temperature. Samples were then buffer-exchanged into 50 mM phosphate, 0.05% LMPG, pH 7.0. Following buffer exchange, samples were bound to Nickel resin in a column, which was then washed with 200 mL of 50 mM phosphate, 0.05% DPC, pH 7.0 to remove unbound MTSL. The spin labeled KCNE3 was eluted using elution buffer (25 mM Tris-HCl, 200 mM NaCl, 250 mM imidazole, pH 7.0) containing 0.5% DPC. The spin labeling efficiency (~75%) was obtained by comparing the nano-drop UV A280 protein concentration with spin concentration obtained from CW-EPR spectroscopy.

Reconstitution into Proteoliposomes

The incorporation of spin-labeled KCNE3 protein into POPC/POPG (3:1) proteoliposomes was obtained by using dialysis methods following a similar protocol described previously

(3, 21–24). The spin labeled KCNE3 protein solubilized in DPC detergent micelles was mixed with a lipid slurry (400 mM SDS, 75 mM POPC and 25 mM POPG, 0.1 mM EDTA, 100mM IMD, pH 7.0). The lipid slurry was pre-equilibrated to transparent mixed micelles using an extensive freeze-thaw cycles. We did more than 20 freeze-thaw cycles to make sure that lipid slurry is homogeneous and transparent. The final molar ratio of protein:lipid was set to 1:400. The mixture of KCNE3-lipid was then applied to extensive dialysis to remove all detergent present. During the dialysis process, KCNE3/POPC/POPG vesicles spontaneously formed. The 4 L dialysis buffer (10 mM imidazole and 0.1 mM EDTA at pH 7.0) was changed two times daily. The complete removal of detergent was determined when the KCNE3-lipid solution became cloudy and the surface tension of the dialysate indicated completion of detergent removal.

Dynamic Light Scattering (DLS) Spectroscopy

Dynamic light scattering (DLS) experiments were performed on a Zetasizer nano series (Malvern Instruments) in disposable 40 μl micro cuvettes at 25 °C. The protein samples reconstituted into POPC/POPG lipid bilayer vesicles were diluted ~5-times with the reconstituted buffer to qualify for DLS experiments. Data were collected for 20 seconds and averaged for 10 scans. A size distribution data based on scattering intensity on a log scale were plotted using Igor Pro (WaveMetrics) software.

CW-EPR Spectroscopy

CW-EPR spectroscopy was carried out on a Bruker EMX X-Band spectrometer at the Ohio Advanced EPR Laboratory at Miami University. Spectra were recorded over a scan width of 100 G with a field modulation of 1 G at a frequency of 100 kHz. Samples were placed in a glass capillary tube (50 μL) with a total protein concentration of approximately 200 μM for micelle samples and 100 μM for proteoliposomes. Each sample was scanned 10 – 20 times with a microwave intensity of 10 mW at 297 K. The side-chain mobility was determined by calculating the inverse central linewidth from each CW-EPR spectrum. The inverse central linewidth provides convenient semi-empirical parameters for the estimation of relative rotational mobility of the nitroxide side-chain (25–28).

An empirical motional parameter (τ_0) was determined from the CW-EPR spectra using equation 1(26, 29–31)

$$\tau_0 = K \times \Delta H \left[\left(\frac{h_0}{h_{-1}} \right)^{1/2} - 1 \right], \quad (1)$$

where, K=6.5 $\times 10^{-10}$ s, ΔH is the width of the center-line, and h_0 and h_{-1} are the heights of the center and high field lines respectively.

CW-EPR Power Saturation Measurements

The CW-EPR spectral lineshapes observed are similar to SDSL-EPR data of membrane proteins reconstituted into lipid bilayers and micelles published in the literature. (32, 33). We next used the accessibility to hydrophobic oxygen to assess the topology of different

segments of KCNE3 within POPC/POPG bilayers. Power saturation experiments were performed on a Bruker EMX X-band CW-EPR spectrometer consisting of an ER 041XG microwave bridge coupled with an ER 4123D CW-Resonator (Bruker BioSpin). Samples were loaded into gas permeable TPX capillary tubes with a total volume of 3 – 4 μl at a concentration of 30 – 50 μM. EPR data collection was carried out using a modulation amplitude of 1 G and varying microwave power of 0.4 – 100 mW. The scan range of all spectra was 90 G, and the final spectra were obtained by signal averaging 5 scans. The power saturation method works on the principle that under non-saturating conditions, the height of the spectral lines is linearly proportional to the square root of the incident microwave power, $P^{1/2}$ (34). If the microwave power is subsequently increased, the increase in signal amplitude becomes less linear with $P^{1/2}$, and signal height starts to decrease as the sample saturates. Nitrogen is used as a control to purge the sample of oxygen and other paramagnetic relaxing agents. The power saturation curves were obtained for the V85C (probe outside of model membrane) and S74C (probe inside of model membrane) on KCNE3 under three conditions: 1. equilibrated with nitrogen as a control; 2. equilibrated with lipid-soluble paramagnetic reagent 20% oxygen (air); and 3. equilibrated with nitrogen in the presence of a water-soluble paramagnetic reagent NiEDDA (2 mM) as previously synthesized (35). The samples were purged with gas for at least 60 minutes at a rate of 10 mL per minute before performing each measurement. High purity nitrogen and house supply compressed air lines were used during the experiment. The resonator remained connected to the gas during all measurements and the sample temperature was held at 297 K. The peak-to-peak amplitude of the first derivative $m_I = 0$ resonance line (A) was measured and plotted against the square root of the incident microwave power. The data points were then fit using a Matlab software script according to equation 2 (34):

$$A = I\sqrt{P}[1 + (2^{\frac{1}{\varepsilon}} - 1)P/P_{\frac{1}{2}}]^{-\varepsilon} \quad (2)$$

where I is a scaling factor, $P_{\frac{1}{2}}$ is the power where the first derivative amplitude is reduced to half of its unsaturated value, and ε is a measure of the homogeneity of saturation of the resonance line. In equation 1, I, ε, and $P_{\frac{1}{2}}$ are adjustable parameters and yield a characteristic $P_{\frac{1}{2}}$ value. The corresponding Φ depth parameters were calculated using equation 3 (34, 36–38).

$$\phi = \ln\left(\frac{\Delta P_{1/2}(O_2)}{\Delta P_{1/2}(NiEDDA)}\right) \quad (3)$$

Where $\Delta P_{1/2}(O_2)$ is the deviation in $P_{1/2}$ values of air and nitrogen interacted samples, and $\Delta P_{1/2}$ (NiEDDA) is the deviation in the $P_{1/2}$ values for NiEDDA and nitrogen interacted samples.

Circular Dichroism Spectroscopy

Circular Dichroism (CD) measurements were performed on an Aviv Circular Dichroism Spectrometer model 435 in a quartz cuvette. The cuvette path length was 1.00 mm. Data were collected from 250 to 190 nm with an average of 3 scans per sample and 1 nm band width at 297 K. Protein samples were prepared in 50 mM NaH_2PO_4 pH 7.0 either with 0.1% DPC or reconstituted into POPC/POPG lipid bilayers. Protein concentrations were held at ~15 μM. When necessary, samples were diluted in 50 mM NaH_2PO_4 buffer at pH 7.0 to minimize the scattering effect. The CD data were analyzed on the Dichroweb website (http://dichroweb.cryst.bbk.ac.uk). A spectral width of 190–240 nm was used during the simulation of CD spectra using Contin-LL with the SMP180 reference set (39–42). All CD data were plotted using Igor software.

RESULTS

Preparation of KCNE3 in Lipid Bilayered Vesicles

In order to study structural dynamics and topology of KCNE3 using EPR spectroscopy, the native cysteine in the KCNE3 amino acid sequence was mutated to serine using site-directed mutagenesis and single cysteine mutants were generated from the cysless vector. POPC/POPG phospholipids were used to obtain optimum homogeneous incorporation of KCNE3 in a lipid bilayer. POPC/POPG lipids are a common mimic for phospholipid bilayers of mammalian cell membrane systems (32, 43, 44). In addition, the gel-to-L_α liquid crystalline phase transition of POPC/POPG is below 0°C (43). The POPC:POPG molar ratio was 3:1, which mimics the level of anionic phospholipids commonly found in mammalian cell membranes (32, 43, 44).

The solvent conditions of the elusion buffer have been optimized to provide optimum vesicle reconstitution. Different detergents including SDS, LMPG, and DPC were tested to elute the protein and mixed the detergent solubilized protein with lipid slurry (lipid slurry preparation is discussed in the method section) and subjected to the dialysis. However, use of DPC as a detergent yielded more homogeneous and stable lipid bilayered vesicle samples for EPR experiments. A previous study utilized SDS detergent for the elution of the protein during the purification (3). The dialysis method employed in this study is a widely accepted method of lipid bilayered vesicles reconstitution in the structure biology field (3, 22, 32, 43–46).

The size and homogeniety of the KCNE3 in lipid bilayered vesicles was examined using dynamic light scattering (DLS) spectroscopy. DLS spectroscopy has been widely used to investigate the size and homogeneity of protein samples (47). The protein sample was diluted with the reconstitution buffer for DLS measurements. During the dilution of the DLS sample, we expect that the concentration of the bilayered vesicle is decreased but the vesicle size is still maintained. Figure 1 shows an illustrative example of the DLS data collected on wild type KCNE3 in POPC/POPG lipid bilayered vesicles. The size of the lipid bilayered vesicle is within the range of 70–90 nm radius.

In order to understand the secondary structural conformation of KCNE3, we performed circular dichroism (CD) spectroscopic measurements on KCNE3 in micelles and lipid bilayered vesicles. CD spectroscopy is a widely utilized biophysical method to study the

overall secondary structure of proteins/peptides(48). Figure 2 shows CD spectra collected on cysless KCNE3 in 0.1% DPC micelles and POPC/POPG lipid bilayered vesicles. Our CD data showed predominant α-helical secondary structures indicated by the peak at 195 nm and troughs at ~208 and ~222 nm. The α-helical content for the liposome sample is higher than that compared for the micelle sample as indicated by greater deep of the spectrum at 222 nm region for liposomes as compared to that for micelles. The quantitative analysis of CD spectral data using Dicroweb website suggested that the helical content of KCNE3 is ~86% in POPC/POPG lipid bilayered vesicles, when compared to that of ~53% in DPC detergent micelles. These CD spectroscopic data also suggested that the folding of KCNE3 is better in the liposomes when compared to that in micelles and hence the study of KCNE3 is required in lipid bilayer environments to better mimic its native like membrane environment.

CW-EPR Spectral Measurements

Site-directed spin labeling EPR spectroscopy (SDSL-EPR) is a powerful biophysical technique to study structural dynamics of membrane proteins(28, 49). Figure 3 shows the chemical structure of MTSL spin label probe and the predicted topology of KCNE3 in lipid bilayers based on previous solution NMR studies(3, 20), and X-Band CW-EPR spectra of spin-labeled KCNE3 mutants in 0.5% DPC micelles and POPC/POPG bilayered vesicles at pH 7.0. The CW-EPR data show a broadening in the spectral linewidths when moving from the micelles to the lipid bilayers and residues in the transmembrane lipid bilayers are more restricted when compared to the residues in the extracellular region of KCNE3. This suggests that the dynamic motion of the nitroxide spin label is lower in the lipid bilayer membrane when compared to the micelles and that lies within the bilayer membrane are less mobile than those outside the bilayer membrane. Similar line broadenings have been previously reported for transmembrane proteins in the literature. (32, 50–53)

In order to quantify the side-chain motion of the spin-labeling sites, the inverse of the central linewidth and the empirical motional parameter (τ_0) were calculated from each spectrum and plotted as a function of the residue number as shown in Figure 4. The inverse central linewidth has been widely used as a powerful semi empirical parameter for the estimation of the relative rotational mobility (25, 27, 54). For the intermediate-to-fast motional regime of EPR having three distinct first-derivative lines, the empirical motional parameter (τ_0) is also known as the rotational correlation time (τ_c) (Figure 4b) (26). The rotational correlation time, τ_c, is the time required for the spin-label to rotate through an angle of one radian. The shorter times (smaller values of τ_c) indicate faster motion. Figure 4a clearly indicates that the spin labeling sites in the TMD of KCNE3 have relatively lower inverse central linewidths when compared to that of the sites in the N- and C-termini. The inverse central linewidth for sites (V85C, and S101C) in the C-terminus of KCNE3 is higher than that for the site S49C in N-terminus of KCNE3. The lower side chain mobility of the site in N-terminus when compared to the site in C-terminus indicates that the N-terminus site may be interacting more closely with the lipid bilayer surface when compared to sites in the C-terminus. The inverse central linewidth data of KCNE3 reported in this study are consistent with previously published NMR studies of KCNE3 and spin-labeled side-chain mobility data for integral membrane proteins (3, 20, 32, 33, 55–57).

The empirical motional parameter (τ_0) provides a quantitative information of the side-chain dynamics of spin-labeled sites of KCNE3. The motional parameter (τ_0) was measured for each residue site according to equation 1. The motional parameter of the TMD of KCNE3 varies from 1.9 ns to 3.5 ns, while the extracellular region varies between 1.1 ns to 2.5 ns. Figure 4b clearly indicates that τ_0 for TMD sites of KCNE3 is higher than that of the sites in extracellular region. The motional parameter pattern for the C-terminus sites is lower when compared to the N-terminus site. The τ_0 parameter values suggest that the spin-labeled KCNE3 TMD side-chains are tumbling slowly when compared to the extracellular termini, with the C-terminus side-chains tumbling faster than the N-terminal sites. This motional parameter pattern is consistent with the spin-label side-chain mobility of the corresponding mutants from Figure 4a.

Power Saturation EPR Measurements for Studying Topology of KCNE3

CW-EPR power saturation experiments are widely used to determine the topology of protein/peptide with respect to membrane bilayers (19, 28, 49). EPR power saturation experiments measure the relaxation rate of spin labels with external paramagnetic probes situated in the solvent phase and in the lipid bilayers by plotting the CW-EPR signal intensity as a function of microwave power (58). Power Saturation EPR experiments were conducted on KCNE3 spin labeled sites V85C (probe outside the bilayer membrane) and S74C (probe inside the bilayer membrane) in lipid bilayered vesicles to confirm the location and insertion of these residues with respect to the membrane. Figure 5 shows the CW-EPR power saturation data for spin labeled sites S74C and V85C of KCNE3. The power saturation curve in Figure 5 reveals that the addition of NiEDDA to V85C KCNE3 has a significant effect on the power saturation curve in POPC/POPG bilayered vesicle. This indicates that V85C is accessible to the solvent. Inspection of the power saturation profile of S74C KCNE3 indicates that the non-polar relaxation probe O_2 in air changes the relaxation profile much greater than both N_2 and polar relaxation probe NiEDDA in POPC/POPG bilayered vesicles, suggesting that site S74C is resided inside the hydrophobic lipid bilayered membrane (3). The N_2 control experiments demonstrated similar saturation patterns for both mutants. The membrane depth parameters (φ) calculated from equation 3 are 1.3±0.3 for S74C and −1.7±0.3 for V85C. The positive φ value reveals that the residue S74C is buried in the bilayer membrane while negative φ value shows the residue V85C is accessible to the solvent (21, 32, 33, 56, 57). The solvent accessibilities of the TMD residue S74C (probe inside the bilayer membrane) and V85C (probe outside the bilayer membrane) of KCNE3 are consistent with the published solution NMR studies of the topology of KCNE3(3, 20). The power saturation data reported in this study are in agreement with the CW-EPR lineshape data (Figure 3C) and side-chain mobility and motional parameters shown in Figure 4.

DISCUSSION

Structural studies of KCNE3 have been previously conducted in a wide range of model membrane mimics (3, 20). It is important to assess the impact of the membrane mimics used on the observed conformation and dynamics. In this paper, we have specifically focused on comparing the conformation and dynamics of KCNE3 in POPC/POPG liposomes and

DPC micelles. For instance, the transmembrane helix of KCNE3 extends from the amino acid residue 57 to 82 in isotropic bilcelles (3). It is important to examine whether the TMD region in the actual lipid bilayered vesicle environment is extended outside the region reported in the isotropic bicelles. Similarly, the helical regions reported for the N- and C-termini need to be examined in the lipid bilayered vesicle environment. The previous DEER data obtained on a pair of spin labeled sites of TMD terminals in POPC/POPG bilayered vesicles suggested that the TMD helix adopts a moderate curvature in bilayer membranes with residues T71, S74, and G78 lie along the concave face of the curvature(3). However, further refinement of the TMD domain is required to obtain in-depth quantitative information of the conformation of the TMD helix. The CW-EPR data for the optimum reconstitution of KCNE3 in POPC/POPG bilayered vesicles reported in this study shows the feasibility of site-directed spin labeling (SDSL) EPR spectroscopic experiments for a detailed examination and refinement of the KCNE3 structure in a bilayered vesicle environment. Recent electrophysiological studies on the cysless form of KCNE3 and KCNQ1 suggested that the site specific cysteine mutation does not significantly perturb the functional activities of the protein(3). Our CD spectroscopic data suggested that KCNE3 is more highly structured in POPC/POPG bilayered vesicles than compared to DPC detergent micelles. The DEER data reported on the KCNE3 in POPC/POPG also suggests a functional preservation of the protein in the POPC/POPG lipid bilayered vesicles(3). Earlier studies on membrane proteins suggested that the method used during the incorporation of the protein into lipid bilayer vesicles is very important to determining the secondary structure of the protein (33, 59–61). Our EPR experimental results are consistent with the CW-EPR spectral lineshape analysis data and power saturation data previously reported on integral membrane proteins(32, 33, 61).

The transmembrane domain (TMD) of KCNE3 is very hydrophobic containing several polar residues on the TMD termini. The polar amino acid residues present on the termini restrain the protein to the polar surface of the membrane while the inner hydrophobic amino acid residues interact with carbon chains of the lipid (3). KCNE3 is insoluble in aqueous solution and tends to aggregate due to its amphipathic behavior. DPC is a zwitterionic detergent belonging to the single chain phospholipids. The presence of DPC in the elution buffer during the reconstitution of KCNE3 utilized in this study keeps this protein in association with relevant concentrations of either detergent or lipids to minimize its interaction with other protein molecules leading to the prevention from the aggregation. The molar ratio of lipid:protein is also significantly higher (400:1) as reported in the literature (3).

CW-EPR power saturation will be very useful technique to determine the association of the specific residues of the helical sections of N-and C-termini of KCNE3 with the lipid bilayered membrane. CW-EPR spectral lineshape analysis and power saturation data will be very helpful to understand how certain residue sites Thr71, Ser74, and Gly78 along the concave face of the curved TMD interact with lipid bilayers. CW-EPR experiments will be very useful to explore how a lipid bilayer could function to stabilize and extend extracellular helical segments, that increases a higher helical content in lipid bilayers than in micelles. Since we have optimized the lipid bilayer sample preparation reported in this study, we will explore the details of the structural topology and conformational dynamics of KCNE3 in our

future studies using the advanced EPR spectroscopic techniques that are utilized for studying membrane proteins.

CONCLUSION

A method for reconstitution of KCNE3 in lipid bilayered vesicles was successfully optimized for EPR spectroscopic studies. Biophysical data on KCNE3 reconstituted into both POPC/POPG liposomes and DPC micelles were reported. The CD spectroscopic data indicate that the structure of KCNE3 in bilayered lipid vesicles is more highly ordered in comparison to that in detergent micelles. The CW-EPR spectral lineshape analysis and power saturation data suggested restricted motion of KCNE3 in lipid bilayered vesicles in comparison to that in detergent micelles. The results of this work will provide guidelines for the further detailed structure and conformational dynamic studies of KCNE3 in more physiological membrane environment using EPR spectroscopy.

Acknowledgments

This work is generously supported by National Science Foundation NSF MCB-2040917 award and Kentucky Academy of Science award. Gary A. Lorigan would like to acknowledge support, NIGMS/NIH Maximizing Investigator's Research Award (MIRA) R35 GM126935 award, the Ohio Board of Regents, and Miami University. Charles R. Sanders would like to acknowledge support from US NIH grant R01 HL122010. Mathew Scheyer would also like to acknowledge support from Appalachian College Association Ledford Scholars Program.

Abbreviations:

CD	Circular Dichroism
CMC	Critical Micelle Concentration
CW	Continuous Wave
DEER	Double Electron-Electron Resonance
DPC	Dodecyl Phosphatidylcholine
EPR	Electron Paramagnetic Resonance
IPTG	Isopropyl β-D-thiogalactopyranoside
LMPG	1-Myristoyl-2-Hydroxy-sn-Glycero-3-Phospho-(1'-rac-Glycerol) (Sodium Salt)\
LMPC	lyso-myristoylphosphatidyl choline
MTSL	(*S*-(2,2,5,5-tetramethyl-2,5-dihydro-1H-pyrrol-3-yl) methyl methanesulfonothioate)
NiEDDA	Nickel(II) ethylenediaminediacetate
DHPC	dihexanoylphosphatidylcholine
DMPG	dimyristoylphosphatidylglycerol

POPC	1-palmitoyl-2-oleoyl-*sn*-glycero-3-phosphocholine
POPG	1-palmitoyl-2-oleoyl-*sn*-glycero-3-phospho-(1'-*rac*-glycerol) (sodium salt)
SDS	Sodium Dodecyl Sulfate
TMD	Transmembrane Domain
WT	Wild Type

References

(1). Schroeder BC, Waldegger S, Fehr S, Bleich M, Warth R, Greger R, and Jentsch TJ (2000) A constitutively open potassium channel formed by KCNQ1 and KCNE3, Nature 403, 196–199. [PubMed: 10646604]

(2). Lewis A, McCrossan ZA, and Abbott GW (2004) MinK, MiRP1, and MiRP2 diversify Kv3.1 and Kv3.2 potassium channel gating, Journal of Biological Chemistry 279, 7884–7892. [PubMed: 14679187]

(3). Kroncke BM, Van Horn WD, Smith J, Kang CB, Welch RC, Song YL, Nannemann DP, Taylor KC, Sisco NJ, George AL, Meiler J, Vanoye CG, and Sanders CR (2016) Structural basis for KCNE3 modulation of potassium recycling in epithelia, Science Advances 2, e1501228. [PubMed: 27626070]

(4). Abbott GW (2016) KCNE1 and KCNE3: The yin and yang of voltage-gated K+ channel regulation, Gene 576, 1–13. [PubMed: 26410412]

(5). Tai KK, and Goldstein SAN (1998) The conduction pore of a cardiac potassium channel, Nature 391, 605–608. [PubMed: 9468141]

(6). Ketchum KA, Joiner WJ, Sellers AJ, Kaczmarek LK, and Goldstein SAN (1995) A new family of outwardly rectifying potassium channel proteins with 2 pore domains in tandem, Nature 376, 690–695. [PubMed: 7651518]

(7). Barro-Soria R, Ramentol R, Liin SI, Perez ME, Kass RS, and Larsson HP (2017) KCNE1 and KCNE3 modulate KCNQ1 channels by affecting different gating transitions, Proc. Natl. Acad. Sci. U. S. A. 114, E7367–E7376. [PubMed: 28808020]

(8). Ohno S, Toyoda F, Zankov DP, Yoshida H, Makiyama T, Tsuji K, Honda T, Obayashi K, Ueyama H, Shimizu W, Miyamoto Y, Kamakura S, Matsuura H, Kita T, and Horie M (2009) Novel KCNE3 Mutation Reduces Repolarizing Potassium Current and Associated With Long QT Syndrome, Human Mutation 30, 557–563. [PubMed: 19306396]

(9). Preston P, Wartosch L, Gunzel D, Fromm M, Kongsuphol P, Ousingsawat J, Kunzelmann K, Barhanin J, Warth R, and Jentsch TJ (2010) Disruption of the K+ Channel beta-Subunit KCNE3 Reveals an Important Role in Intestinal and Tracheal Cl- Transport, Journal of Biological Chemistry 285, 7165–7175. [PubMed: 20051516]

(10). Boucherot A, Schreiber R, and Kunzelmann K (2001) Regulation and properties of KCNQ1 (K(v)LQT1) and impact of the cystic fibrosis transmembrane conductance regulator, Journal of Membrane Biology 182, 39–47. [PubMed: 11426298]

(11). Lundby A, Ravn LS, Svendsen JH, Haunso S, Olesen SP, and Schmitt N (2008) KCNE3 mutation V17M identified in a patient with lone atrial fibrillation, Cellular Physiology and Biochemistry 21, 47–54. [PubMed: 18209471]

(12). Abbott GW, Butler MH, and Goldstein SAN (2006) Phosphorylation and protonation of neighboring MiRP2 sites: function and pathophysiology of MiRP2-Kv3.4 potassium channels in periodic paralysis, Faseb Journal 20, 293–301. [PubMed: 16449802]

(13). Delpon E, Cordeiro JM, Nunez L, Thomsen PEB, Guerchicoff A, Pollevick GD, Wu YS, Kanters JK, Larsen CT, Burashnikov E, Christiansen M, and Antzelevitch C (2008) Functional Effects of KCNE3 Mutation and Its Role in the Development of Brugada Syndrome, Circulation-Arrhythmia and Electrophysiology 1, 209–218. [PubMed: 19122847]

(14). Zhang DF, Liang B, Lin J, Liu B, Zhou QS, and Yang YQ (2005) KCNE3 R53H substitution in familial atrial fibrillation, Chinese Medical Journal 118, 1735–1738. [PubMed: 16313760]

(15). Sun J, and MacKinnon R (2020) Structural Basis of Human KCNQ1 Modulation and Gating, Cell 180, 1–8. [PubMed: 31836194]

(16). Kasuya G, and Nakajo K (2021) Triad interaction stabilizes the voltage sensor domains in a constitutively open KCNQ1 - KCNE3 channel, bioRxiv, April 06.

(17). Page RC, Li C, Hu J, Gao FP, and Cross TA (2007) Lipid bilayers: an essential environment for the understanding of membrane proteins, Magnetic Resonance in Chemistry 45, S2–S11. [PubMed: 18095258]

(18). Yeh V, Goode A, and Bonev BB (2020) Membrane Protein Structure Determination and Characterisation by Solution and Solid-State NMR, Biology-Basel 9, 396. [PubMed: 33198410]

(19). Sahu ID, and Lorigan GA (2021) Probing structural dynamics of membrane proteins using electron paramagnetic resonance spectroscopic techniques, Biophysica 1, 106–125.

(20). Kang CB, Vanoye CG, Welch RC, Van Horn WD, and Sanders CR (2010) Functional Delivery of a Membrane Protein into Oocyte Membranes Using Bicelles, Biochemistry 49, 653–655. [PubMed: 20044833]

(21). Barrett PJ, Song Y, Van Horn WD, Hustedt EJ, Schafer JM, Hadziselimovic A, Beel AJ, and Sanders CR (2012) The Amyloid Precursor Protein Has a Flexible Transmembrane Domain and Binds Cholesterol, Science 336, 1168–1171. [PubMed: 22654059]

(22). Sahu ID, Kroncke BM, Zhang R, Dunagan MM, Smith HJ, Craig A, McCarrick RM, Sanders CR, and Lorigan GA (2014) Structural Investigation of the Transmembrane Domain of KCNE1 in Proteoliposomes, Biochemistry 53, 6392–6401. [PubMed: 25234231]

(23). Sahu ID, McCarrick RM, Troxel KR, Zhang R, Smith HJ, Dunagan MM, Swartz MS, Rajan PV, Kroncke BM, Sanders CR, and Lorigan GA (2013) DEER EPR measurements for membrane protein structures via bifunctional spin labels and lipodisq nanoparticles, Biochemistry 52, 6627–6632. [PubMed: 23984855]

(24). Sahu ID, Dixit G, Reynolds WD, Kaplevatsky R, Harding BD, Jaycox CK, McCarrick RM, and Lorigan GA (2020) Characterization of the Human KCNQ1 Voltage Sensing Domain (VSD) in Lipodisq Nanoparticles for Electron Paramagnetic Resonance (EPR) Spectroscopic Studies of Membrane Proteins, Journal of Physical Chemistry B 124, 2331–2342. [PubMed: 32130007]

(25). Hubbell WL, McHaourab HS, Altenbach C, and Lietzow MA (1996) Watching proteins move using site-directed spin labeling, Structure 4, 779–783. [PubMed: 8805569]

(26). Klug CS, and Feix JB (2008) Methods and Applications of Site-Directed Spin Labeling EPR Spectroscopy, Methods Cell Biol. 84, 617–658. [PubMed: 17964945]

(27). Hubbell WL, Cafiso DS, and Altenbach C (2000) Identifying conformational changes with site-directed spin labeling, Nature Structural Biology 7, 735–739. [PubMed: 10966640]

(28). Sahu ID, McCarrick RM, and Lorigan GA (2013) Use of Electron Paramagnetic Resonance to Solve Biochemical Problems, Biochemistry 52, 5967–5984. [PubMed: 23961941]

(29). Bates IR, Boggs JM, Feix JB, and Harauz G (2003) Membrane-anchoring and charge effects in the interaction of myelin basic protein with lipid bilayers studied by site-directed spin labeling, Journal of Biological Chemistry 278, 29041–29047. [PubMed: 12748174]

(30). Boggs JM, and Moscarello MA (1978) Effect of basic-protein from human central nervous-system myelin on lipid bilayer structure, Journal of Membrane Biology 39, 75–96. [PubMed: 204786]

(31). Eletr S, and Keith AD (1972) Spin-label studies of dynamics of lipid alkyl chains in biological-membranes - role of unsaturated sites, Proceedings of the National Academy of Sciences of the United States of America 69, 1353–1357. [PubMed: 4338592]

(32). Sahu ID, Craig AF, Dunagan MM, Troxel KR, Zhang R, Meiberg AG, Harmon CN, MaCarrick RM, Kroncke BM, Sanders CR, and Lorigan GA (2015) Probing Structural Dynamics and Topology of the KCNE1 Membrane Protein in Lipid Bilayers via Site-Directed Spin Labeling and Electron Paramagnetic Resonance Spectroscopy, Biochemistry 54, 6402–6412. [PubMed: 26418890]

(33). Dixit G, Sahu ID, Reynolds WD, Wadsworth TM, Harding BD, Jaycox CK, Dabney-Smith C, Sanders CR, and Lorigan GA (2019) Probing the Dynamics and Structural Topology

of the Reconstituted Human KCNQ1 Voltage Sensor Domain (Q1-VSD) in Lipid Bilayers Using Electron Paramagnetic Resonance Spectroscopy, Biochemistry 58, 965–973. [PubMed: 30620191]

(34). Altenbach C, Greenhalgh DA, Khorana HG, and Hubbell WL (1994) A collision gradient method to determine the immersion depth of nitroxides in lipid bilayers: application to spin-labeled mutants of bacteriorhodopsin, Proc Natl Acad Sci U S A 91, 1667–1671. [PubMed: 8127863]

(35). Averill DF, Smith DL, and Legg JI (1972) 5-Coordinate, Square-Pyramidal Chelate Complexes of a Novel Tetradentate Amino-Acid Like Ligand, Inorg Chem 11, 2344–2349.

(36). Rauch ME, Ferguson CG, Prestwich GD, and Cafiso DS (2002) Myristoylated alanine-rich C kinase substrate (MARCKS) sequesters spin-labeled phosphatidylinositol 4,5-bisphosphate in lipid bilayers, J Biol Chem 277, 14068–14076. [PubMed: 11825894]

(37). Frazier AA, Wisner MA, Malmberg NJ, Victor KG, Fanucci GE, Nalefski EA, Falke JJ, and Cafiso DS (2002) Membrane orientation and position of the C2 domain from cPLA2 by site-directed spin labeling, Biochemistry 41, 6282–6292. [PubMed: 12009889]

(38). Kohout SC, Corbalan-Garcia S, Gomez-Fernandez JC, and Falke JJ (2003) C2 domain of protein kinase C alpha: elucidation of the membrane docking surface by site-directed fluorescence and spin labeling, Biochemistry 42, 1254–1265. [PubMed: 12564928]

(39). Miles AJ, Ramalli SG, and Wallace BA (2022) DichroWeb, a website for calculating protein secondary structure from circular dichroism spectroscopic data, Protein Science 31, 37–46. [PubMed: 34216059]

(40). Whitmore L, and Wallace BA (2008) Protein secondary structure analyses from circular dichroism spectroscopy: Methods and reference databases, Biopolymers 89, 392–400. [PubMed: 17896349]

(41). Vanstokkum IHM, Spoelder HJW, Bloemendal M, Vangrondelle R, and Groen FCA (1990) Estimation of protein secondary structure and error analysis from circular-dichroism spectra, Analytical Biochemistry 191, 110–118. [PubMed: 2077933]

(42). Abdul-Gader A, Miles AJ, and Wallace BA (2011) A reference dataset for the analyses of membrane protein secondary structures and transmembrane residues using circular dichroism spectroscopy, Bioinformatics 27, 1630–1636. [PubMed: 21505036]

(43). Barrett PJ, Song Y, Van Horn WD, Hustedt EJ, Schafer JM, Hadziselimovic A, Beel AJ, and Sanders CR (2012) The Amyloid Precursor Protein Has a Flexible Transmembrane Domain and Binds Cholesterol, Science 336, 1168–1171. [PubMed: 22654059]

(44). Song Y, Hustedt EJ, Brandon S, and Sanders CR (2013) Competition Between Homodimerization and Cholesterol Binding to the C99 Domain of the Amyloid Precursor Protein, Biochemistry 52, 5051–5064. [PubMed: 23865807]

(45). Sahu ID, Zhang R, Dunagan MM, Craig A, and A., L. G. (2017) Characterization of KCNE1 inside lipodisq nanoparticles for EPR spectroscopic studies of membrane proteins, J Phys. Chem. B 121, 5312–5321. [PubMed: 28485937]

(46). Sahu ID, Craig AF, Dunagum MM, McCarrick RM, and Lorigan GA (2017) Characterization of bifunctional spin labels for investigating the structural and dynamic properties of membrane proteins using EPR spectroscopy, Journal of Physical Chemistry B 121, 9185–9195. [PubMed: 28877443]

(47). Stetefeld J, McKenna SA, and Patel TR (2016) Dynamic light scattering: a practical guide and applications in biomedical sciences, Biophys Rev. 8, 409–427. [PubMed: 28510011]

(48). Miles AJ, and Wallace BA (2016) Circular dichroism spectroscopy of membrane proteins, Chemical Society Reviews 45, 4859–4872. [PubMed: 27347568]

(49). Sahu ID, and Lorigan GA (2020) Electron paramagnetic resonance as a tool for studying membrane proteins, Biomolecules 10, 763. [PubMed: 32414134]

(50). Pohl T, Spatzal T, Aksoyoglu M, Schleicher E, Rostas AM, Lay H, Glessner U, Boudon C, Hellwig P, Weber S, and Friedrich T (2010) Spin labeling of the Escherichia coli NADH ubiquinone oxidoreductase (complex I), Biochim Biophys Acta 1797, 1894–1900. [PubMed: 20959113]

(51). Klug CS, Su W, and Feix JB (1997) Mapping of the residues involved in a proposed beta-strand located in the ferric enterobactin receptor FepA using site-directed spin-labeling, Biochemistry 36, 13027–13033. [PubMed: 9335564]

(52). Naber N, Rice S, Matuska M, Vale RD, Cooke R, and Pate E (2003) EPR spectroscopy shows a microtubule-dependent conformational change in the kinesin switch 1 domain, Biophys J 84, 3190–3196. [PubMed: 12719248]

(53). Glasgow BJ, Gasymov OK, Abduragimov AR, Yusifov TN, Altenbach C, and Hubbell WL (1999) Side chain mobility and ligand interactions of the G strand of tear lipocalins by site-directed spin labeling, Biochemistry 38, 13707–13716. [PubMed: 10521278]

(54). Hubbell WL, Gross A, Langen R, and Lietzow MA (1998) Recent advances in site-directed spin labeling of proteins, Curr. Opinion Struct. Biol. 8, 649–656.

(55). Li Q, Wanderling S, Sompornpisut P, and Perozo E (2014) Structural basis of lipid-driven conformational transitions in the KvAP voltage-sensing domain, Nature Structural & Molecular Biology 21, 160–166.

(56). Ahammad T, Drew DL Jr., Sahu ID, Serafin RA, Clowes KR, and Lorigan GA (2019) Continuous Wave Electron Paramagnetic Resonance Spectroscopy Reveals the Structural Topology and Dynamic Properties of Active Pinholin $S2^{16}8$ in a Lipid Bilayer, J. Phys. Chem. B 123, 8048–8056. [PubMed: 31478671]

(57). Ahammad T, Drew DL, Khan RH, Sahu ID, Faul E, Li T, and Lorigan GA (2020) Structural Dynamics and Topology of the Inactive Form of S21 Holin in a Lipid Bilayer Using Continuous-Wave Electron Paramagnetic Resonance Spectroscopy, J. Phys. Chem. B 124, 5370–5379. [PubMed: 32501696]

(58). Altenbach C, Greenhalgh DA, Khorana HG, and Hubbell WL (1994) A Collision Gradient Method to Determine the Immersion Depth of Nitroxides in Lipid Bilayers: Application to Spin-Labeled Mutants of Bacteriorhodopsin, Proc. Natl. Acad. Sci. U.S.A. 91, 1667–1671. [PubMed: 8127863]

(59). Aggeli A, Bannister ML, Bell M, Boden N, Findlay JBC, Hunter M, Knowles PF, and Yang JC (1998) Conformation and ion-channeling activity of a 27-residue peptide modeled on the single-transmembrane segment of the IsK (minK) protein, Biochemistry 37, 8121–8131. [PubMed: 9609707]

(60). Mercer EAJ, Abbott GW, Brazier SP, Ramesh B, Haris PI, and Srai SKS (1997) Synthetic putative transmembrane region of minimal potassium channel protein (minK) adopts an alpha-helical conformation in phospholipid membranes, Biochem J 325, 475–479. [PubMed: 9230130]

(61). Coey AT, Sahu ID, Gunasekera TS, Troxel KR, Hawn JM, Swartz MS, Wickenheiser MR, Reid RJ, Welch RC, Vanoye CG, Kang CB, Sanders CR, and Lorigan GA (2011) Reconstitution of KCNE1 into lipid Bilayers: comparing the structural, dynamic, and activity differences in micelle and vesicle environments, Biochemistry 50, 10851–10859. [PubMed: 22085289]

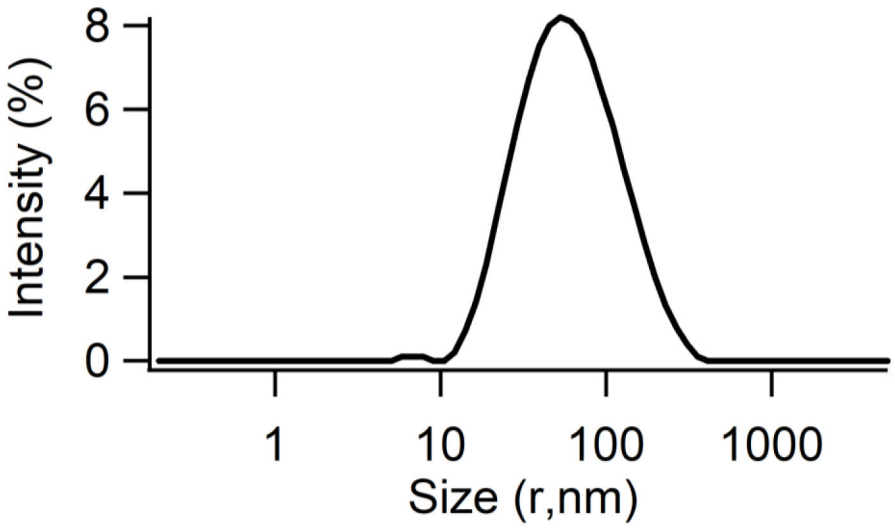

Figure 1:
An illustrative example of the DLS data of wild type KCNE3 incorporated into the POPC/POPG proteoliposomes. Signal intensity is plotted as a log function of particle radius.

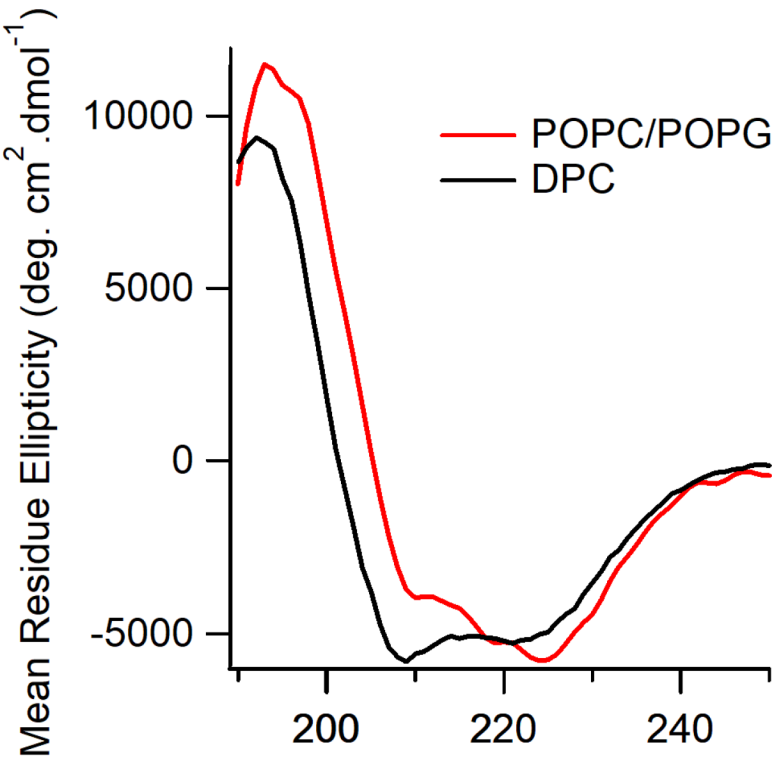

Figure 2.

CD spectra of Cysteine reduced KCNE3 in micelle and vesicle environments. **Black**, 0.1% DPC micelles, **Red**, POPC/POPG MLVs, 400:1=Lipid:Protein ratio, pH 7.0 at 297 K.

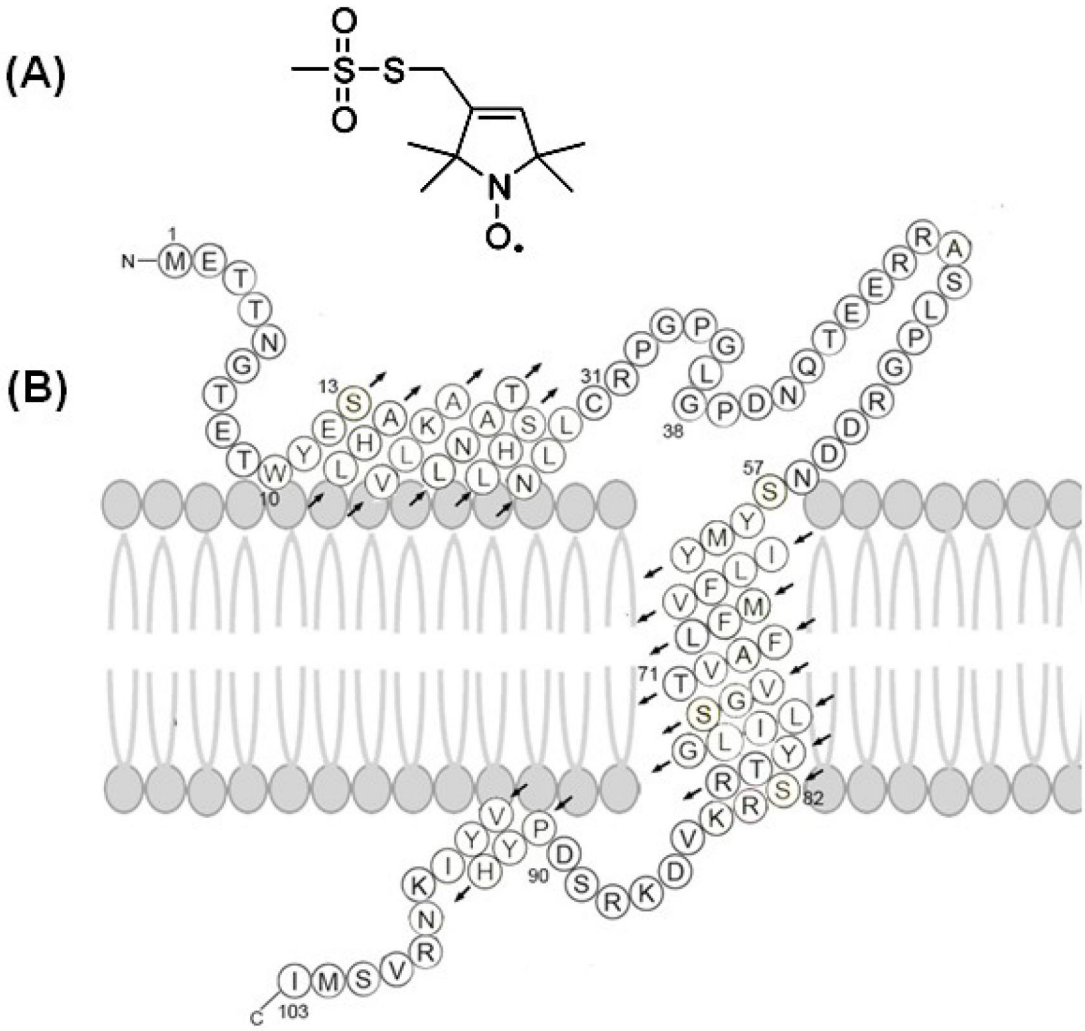

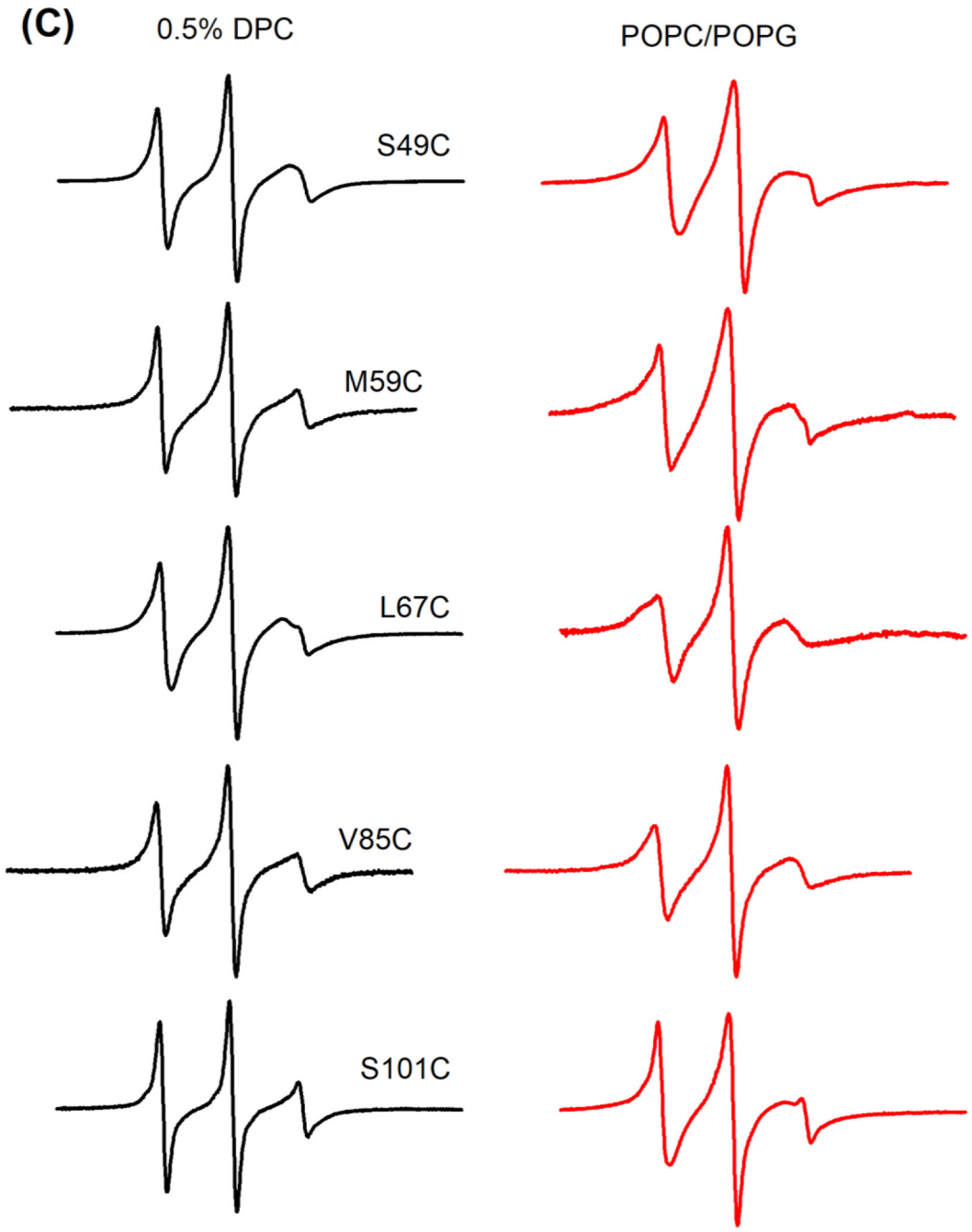

Figure 3:

(**A**) Chemical structure of the MTSL spin label probe, **(B)** a predicted topology of KCNE3 in lipid bilayers based on previous solution NMR studies(3, 20), **(C)** CW-EPR spectra on KCNE3 mutants in 0.5% DPC micelles (left panel) and POPC/POPG bilayered vesicles (right panel). Spectra were normalized to the highest intensity of the spectrum.

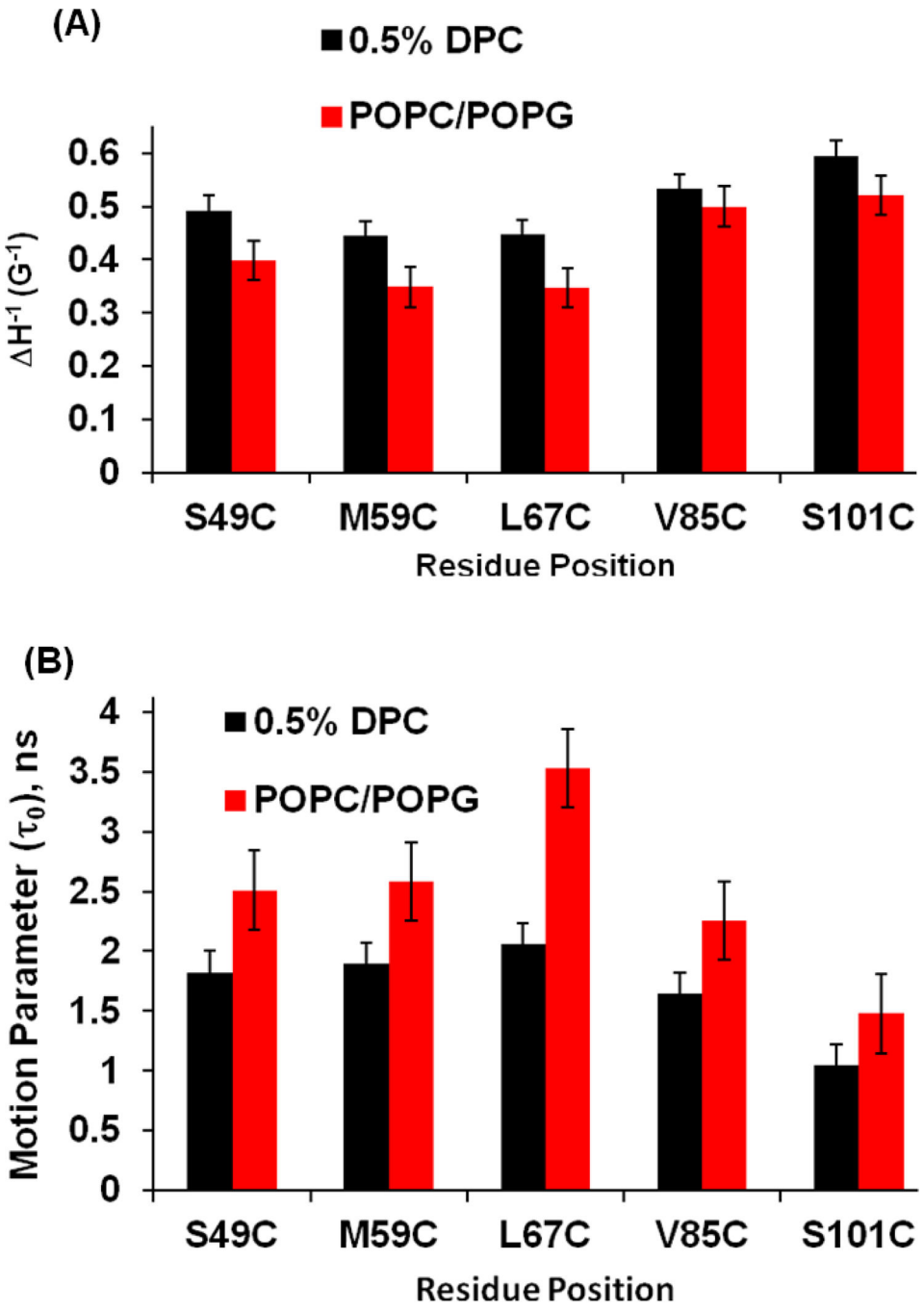

Figure 4:

(A) Plot of the inverse central EPR resonance linewidth (m_I=0) as a function of residue position, as calculated from the CW-EPR spectra of KCNE3 mutants shown in Figure 3C. **(B)** Plot of the motional parameter (τ_0) as a function of residue position calculated from the CW-EPR spectra of KCNE3 mutants shown in Figure 3C.

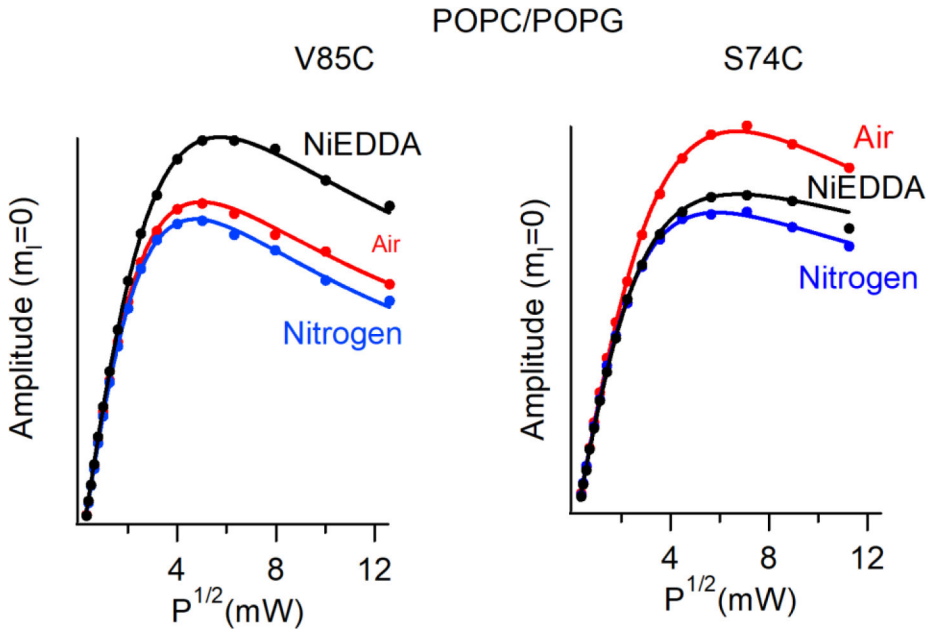

Figure 5.

EPR Power saturation curves for KCNE3 in POPC/POPG bilayered vesicles at pH 7.0, 297 K. Mutation V85C is outside the lipid bilayer and mutation S74C is part of the transmembrane domain (TMD).